



Oxidative stress-induced decreased expression of FABP5 leads to mitochondrial damage and survival disorder of decidual stromal cells in women with recurrent spontaneous abortion

Dong Li^{a,***,1}, Honglei Duan^{a,1}, Zihan Jiang^a, Chunxiang Zhou^a, Chenrui Cao^a, Mengyao Ni^a, Linlin He^a, Xiangyu Zhu^a, Liang Jin^a, Wei Liu^a, Leilei Gu^a, Huijun Li^a, Dan Liu^a, Xiaolei Zhao^{a,b}, Guangfeng Zhao^{a,**}, Jie Li^{a,b,*}

^a Department of Obstetrics and Gynecology, Nanjing Drum Tower Hospital, Affiliated Hospital of Medical School, Nanjing University, 210000, Nanjing, China

^b Nanjing Drum Tower Hospital Clinical College of Nanjing Medical University, 210000, Nanjing, China

ARTICLE INFO

Keywords:

FABP5
decidual stromal cells
Apoptosis
Mitochondria
MRPL17

ABSTRACT

Background: The survival of decidual stromal cells (DSCs) at the maternal-fetal interface is critical for maintaining pregnancy. Dysfunction of DSCs is a significant contributor to recurrent spontaneous abortion (RSA), though the precise regulatory mechanisms remain elusive. Here, we report a marked downregulation of fatty acid-binding protein 5 (FABP5) in decidual tissues and DSCs from RSA donors, suggesting its potential role in RSA pathogenesis.

Methods: Using decidual tissues and DSCs from normal pregnancy (NP) and RSA donors, we quantified FABP5 expression via qPCR, Western blot, immunofluorescence, and immunohistochemistry. Cellular viability and apoptosis were assessed through CCK8 assays, Ki67 staining, flow cytometry, and TUNEL assays. Mitochondrial integrity and function were evaluated by JC-1 staining, COXIV immunostaining, and ATP quantification. RNA sequencing (RNA-seq) identified downstream targets of FABP5. The migratory and invasive capacities of human extravillous trophoblast cells line (HTR-8/SVneo) were examined via wound healing and transwell assays.

Results: FABP5 expression was significantly reduced in decidual tissues and DSCs from RSA donors, as well as in tert-butyl hydroperoxide (TBHP)-induced oxidative stress models *in vitro*. siRNA-mediated FABP5 knockdown triggered mitochondrial dysfunction and apoptosis in DSCs, mechanistically linked to mitochondrial ribosomal protein L17 (MRPL17), a pivotal regulator of oxidative respiratory chain enzyme complex synthesis. MRPL17 overexpression alleviated these effects. Furthermore, FABP5 deficiency suppressed CXCL11 secretion, leading to diminished CXCR3 levels in HTR-8/SVneo cells and impairing their migration and invasion.

Conclusions: Our findings demonstrate that FABP5 downregulation compromises DSC survival by disrupting MRPL17-dependent mitochondrial function, thereby attenuating CXCL11/CXCR3 mediated trophoblast invasion and migration. This study unveils a novel FABP5/MRPL17/CXCL11/CXCR3 axis in RSA pathogenesis, highlighting FABP5 as a potential therapeutic target for pregnancy maintenance.

1. Introduction

Recurrent spontaneous abortion (RSA), defined as two or more consecutive pregnancy losses before 28 weeks of gestation, represents a

complex disorder with multifactorial etiology [1,2]. While established causes include genetic abnormalities, uterine malformations, and endocrine disorders, approximately 50 % of cases remain unexplained [2,3]. Emerging evidence highlights endometrial dysfunction as a

* Corresponding author. Department of Obstetrics and Gynecology, Nanjing Drum Tower Hospital, Affiliated Hospital of Medical School, Nanjing University, 210000, Nanjing, China.

** Corresponding author.

*** Corresponding author.

E-mail addresses: ericlee890915@163.com (D. Li), zhaoguangfeng@njgly.com (G. Zhao), Jie1967@126.com (J. Li).

¹ Dong Li and Honglei Duan contributed equally to this work.

critical contributor to RSA pathogenesis [3], underscoring the importance of investigating its cytological and molecular mechanisms to better understand RSA pathogenesis.

Decidual stromal cells (DSCs), the predominant cell type in the maternal decidua during pregnancy, are essential for embryo implantation, placentation, and fetal development through cytokines and chemokines secretion [4–6]. However, DSC dysfunction, including abnormal apoptosis or premature senescence, can disrupt maternal-fetal interface and contribute to pregnancy loss [7–10].

Oxidative stress, characterized by an imbalance between reactive oxygen species (ROS) and antioxidant defenses, has been implicated in RSA pathogenesis [11–14]. Although physiological oxidative stress occurs during early pregnancy, proper placental development normally restores redox balance through antioxidant enzyme upregulation [14, 15]. In contrast, RSA patients exhibit persistent oxidative stress in decidual tissues, as evidenced by decreased superoxide dismutase activity, elevated lipid peroxidation [16], and aberrant ROS accumulation with reduced heme oxygenase-1 (HO-1, encoded by HMOX1) expression in DSCs [17]. These findings indicate that sustained oxidative damage in DSCs may underlie endometrial dysfunction in RSA, though the precise mechanisms require further elucidation.

Fatty acid-binding protein 5 (FABP5), a key lipid chaperone, regulates cellular proliferation and apoptosis by facilitating fatty acid transport and metabolism [18,19]. Under oxidative stress conditions, FABP5 dysregulation can lead to mitochondrial dysfunction [20–22], though its role in RSA remains unclear. In this study, we investigated how FABP5 deficiency contributes to DSC impairment and RSA pathogenesis.

Our findings demonstrate that RSA-associated DSCs exhibit increased apoptosis and oxidative stress alongside reduced FABP5 expression. *In-vitro* studies using tert-butyl hydroperoxide (TBHP)-treated DSCs recapitulated these observations. Mechanistically, FABP5 knockdown impaired DSC survival and mitochondrial function through MRPL17, a critical regulator of mitochondrial respiratory chain complexes I (mitochondrially encoded NADH dehydrogenase subunit 2 [MT-ND2]), mitochondrially encoded NADH dehydrogenase subunit 4 [MT-ND4], mitochondrially encoded NADH dehydrogenase subunit 4L [MT-ND4L], III (Cytochrome B [CYTB]), and IV (mitochondrially encoded cytochrome c oxidase subunit III [MT-CO3]). Furthermore, FABP5 deficiency disrupted CXCL11/CXCR3 signaling between DSCs and trophoblasts, ultimately impairing trophoblast migration and invasion. These results establish FABP5 as a crucial regulator of decidual homeostasis, with its dysfunction contributing to RSA through mitochondrial impairment and compromised maternal-fetal crosstalk.

2. Materials and methods

2.1. Patients and sample collection

Decidual tissues were collected from individuals with normal pregnancy (NP) who opted for induced abortion for personal reasons, as well as from patients with RSA who had experienced two or more spontaneous abortions (including the current one).

The exclusion criteria were as follows: (1) severe immediate allergic reactions to any drug; (2) severe endometriosis, uterine fibroids, uterine malformations, intrauterine adhesions, or thin endometrium; (3) abnormal karyotype in either parents or the aborted fetus; (4) comorbid autoimmune diseases, such as systemic lupus erythematosus (SLE), among others; (5) abnormal coagulation, liver and kidney function, or other underlying conditions (e.g., uncontrolled hypertension, diabetes mellitus, thyroid disease, sexually transmitted diseases.) that, in the investigator's opinion, could interfere with the study. Basic patient information is presented in Table 1.

Table 1

Detailed information of the RSA and NP patients.

Parameters	NP (n = 21)	RSA(n = 13)	P value
Maternal age (year)	30.524 ± 6.022	29.308 ± 1.797	0.4858
Gestation age (weeks)	6.857 ± 0.655	7.308 ± 0.947	0.1103
Number of pregnancies	2.619 ± 1.830	2.692 ± 1.032	0.8962
Number of live births	0.714 ± 0.644	0.000 ± 0.000	0.0004
Number of spontaneous abortion	0.143 ± 0.359	2.385 ± 0.650	<0.0001

Note: Values are presented as mean ± SEM.

Abbreviation: NP, normal pregnancy; RSA, recurrent spontaneous abortion.

2.2. Isolation and culture of cells

The isolation of primary DSCs from NP and RSA donors was performed according to the protocol outlined by Liang et al. [7]. Briefly, the procedure is as follows: the decidual tissue was chopped into small pieces and digested at 37 °C for 1.5 h with 1 mg/ml type VI collagenase (Merck, Darmstadt, Germany, CAT#C4-28). After digestion, the cell suspension was sequentially filtered through 100 µm and 40 µm cell strainers and then neutralized with DMEM/F12 culture medium (Multicell, Dallas, Texas, USA, CAT# 319-006-CL) supplemented with 10 % (v/v) fetal bovine serum (FBS) (Bio-Channel, Nanjing, Jiangsu, China, CAT# BC-SE-FBS01). The suspension was centrifuged at 1,000 rpm for 5 min, washed, and centrifuged again before being resuspended in DMEM/F12 complete medium containing 10 % (v/v) FBS, 100 U/ml penicillin, and 100 µg/ml streptomycin (Multicell, CAT# 450-201-EL). The cells were then seeded into a 100 cm² dish and incubated at 37 °C in a 5 % CO₂ atmosphere.

HTR-8/Svneo cells, originally purchased from Wuhan Pricella Biotechnology Co., Ltd and maintained in our laboratory, were utilized in the cell culture experiments. The cells were cultured in RPMI 1640 medium (Gibco, California, USA, CAT# C11875500BT) supplemented with 10 % (v/v) FBS, 100 U/ml penicillin, and 100 mg/ml streptomycin. The cells were maintained in an incubator at 37 °C with a 5 % CO₂ atmosphere.

2.3. Plasmid construction and siRNA transfection

The Flag-tagged MRPL17 expression vector was constructed by Jinzai Biotechnology Co., Ltd. (Nanjing, Jiangsu, China). FABP5-targeting, MRPL17-targeting siRNAs, and CXCR3-targeting siRNAs, along with the negative control (NC) siRNA, were synthesized by Shanghai Gene-Pharma Co., Ltd. (Shanghai, China). The use of siRNAs is shown in Table 2.

The FABP5-targeting siRNA, MRPL17-targeting siRNA and the Flag-tagged MRPL17 expression vector were transfected into DSCs using Lipofectamine™ 3000 Transfection Reagent (Thermo Fisher Scientific, Waltham, Massachusetts, USA, CAT# L3000015), while CXCR3-targeting siRNA was transfected into HTR-8/Svneo cells. The transfection procedure was performed according to the manufacturer's instructions. After 48 h, the transfected DSCs were used for subsequent experiments.

2.4. Immunohistochemistry

Decidual tissues were fixed in a 10 % (v/v) formalin/PBS solution. Paraffin-embedded sections of the tissues were deparaffinized and rehydrated, followed by quenching of endogenous peroxidase activity using 0.3 % H₂O₂. Antigen retrieval was performed by autoclaving the sections in an EDTA solution (pH = 9.0). Afterward, the sections were incubated in a blocking solution for 30 min to inhibit endogenous biotin activity. The samples were then incubated with a primary antibody at 4 °C overnight. After rinsing with TBST, the sections were treated with a horseradish peroxidase-conjugated secondary antibody (Typing, Guangzhou, Guangdong, China, CAT# TPB-0015) at room temperature

Table 2
siRNAs sequences.

Gene	Forward (5'–3')	Reverse (5'–3')
<i>FABP5</i>	UGGGAAGGAAAGCACAUAATT	UAUUGUGCUUCCUCCATT
<i>MRPL17</i>	CGGAGAAGCUCAUCGACUAUGGGAA	UUCCCAUAGUCGAUHAUCUCCG
<i>CXCR3</i>	AGGAGCUGCUCAGAGUAAUACACAG	CUGUGAUUACUCUGAGCAGUCCU
Negative control	UUCUCCGAACGUGUCACGUTT	ACGUGACACGUUCGGAGAATT

for 8 min. Signals were visualized using diaminobenzidine (DAB) (Typing, CAT# TPB-0013) as the chromogen and counterstained with hematoxylin. Finally, the sections were examined under a microscope (Leica DM6B). The use of antibodies is shown in Table 3.

Table 3
Antibody information list.

Antibodies	Source (Catalog number)	Dilution ratio	Use
BAX Polyclonal antibody	ProteinTech (50599-2-Ig)	WB	1:1000
BCL2 Ab	Abways (CY6717)	WB	1:1000
Cleaved Caspase 3; p17 Monoclonal antibody	ProteinTech (68773-1-Ig)	IF	1:200
Cleaved Caspase 3 Polyclonal antibody	ProteinTech (25128-1-AP)	WB	1:500
Cytochrome C Monoclonal antibody	ProteinTech (66264-1-Ig)	WB	1:1000
Vimentin Polyclonal antibody	ProteinTech (10366-1-AP)	IF	1:200
Anti-Vimentin	Abcam (ab8978)	IF	1:200
FABP5 Polyclonal antibody	ProteinTech (12348-1-AP)	WB	1:1000
FABP5 Monoclonal antibody	ProteinTech (66299-1-Ig)	IF/IHC	1:200
HO-1/HMOX1 Polyclonal antibody	ProteinTech (10701-1-AP)	WB	1:1000
NQO1 Polyclonal antibody	ProteinTech (11451-1-AP)	WB	1:1000
HRP-conjugated GAPDH Mouse mAb	Abclonal (AC035)	WB	1:8000
HRP-conjugated β -Actin Rabbit mAb	Abclonal (AC028)	WB	1:8000
COXIV Polyclonal antibody	ProteinTech (11242-1-AP)	IF	1:200
MRPL17 Polyclonal Antibody	Invitrogen (PA5-103521)	IF/WB	1:200/ 1:500
MT-ND4 polyclonal antibody	ProteinTech (26736-1-AP)	WB	1:1000
CYTB polyclonal antibody	ProteinTech (55090-1-AP)	WB	1:2000
MT-CO3 polyclonal antibody	Bioworld (BS71772)	WB	1:1000
MMP-2 (D4M2N) Rabbit mAb	Cell Signaling Technology (40994)	WB	1:1000
CXCL11 Rabbit monoclonal antibody	Bioworld (BS40750)	WB	1:500
CXCR3 Polyclonal antibody	ProteinTech (26756-1-AP)	WB	1:1000
Fluorescein (FITC) AffiniPure™ Goat Anti-Mouse IgG (H + L)	Jackson ImmunoResearch (115-095-003)	IF	1:200
Rhodamine (TRITC) AffiniPure™ Goat Anti-Rabbit IgG (H + L)	Jackson ImmunoResearch (111-025-045)	IF	1:200
Alexa Fluor® 488 AffiniPure™ Goat Anti-Rabbit IgG (H + L)	Jackson ImmunoResearch (111-545-003)	IF	1:200
Alexa Fluor® 647 AffiniPure™ Goat Anti-mouse IgG (H + L)	Jackson ImmunoResearch (111-605-003)	IF	1:200
Anti-mouse IgG HRP-linked Antibody	Cell Signaling Technology (7076)	WB	1:2000
Anti-rabbit IgG HRP-linked Antibody	Cell Signaling Technology (7074)	WB	1:2000

2.5. Immunofluorescence

Paraffin-embedded sections of decidual tissues underwent standard immunohistochemistry processing before incubation with the secondary antibody at room temperature for 1 h. After washing with TBST, the slides were mounted using a DAPI-containing mounting medium (Abcam, Cambridge, United Kingdom; CAT# Ab140139).

DSCs were cultured in 24-well plates, each containing a pre-positioned cell climber (14 mm in diameter). The cells were fixed at room temperature for 30 min using either 4 % (w/v) paraformaldehyde (PFA) or pre-chilled methanol (−20 °C). After fixation, the cells were permeabilized with 0.1 % (v/v) Triton X-100 in PBS for 15 min and then blocked with 3 % (g/v) BSA in PBS. The cells were incubated overnight at 4 °C with a primary antibody. Following PBS washes, they were treated with fluorescence-conjugated secondary antibodies for 1 h at room temperature. The cell climbers were then inverted onto slides using a DAPI-containing mounting medium. Finally, the samples were observed under a fluorescence microscope (Leica DM6B, Wetzlar, Germany) in the dark. The use of antibodies is shown in Table 3.

2.6. Western blotting analysis

Decidual tissues and cells were rinsed twice with cold PBS and lysed directly using a cell lysis solution to extract proteins. Protein concentrations were determined using a BCA Protein Assay Kit (Thermo Fisher Scientific; CAT# 23225). Equal amounts of total protein were subjected to western blotting following standard protocols. Immunoblotting was performed using primary antibodies, either incubated overnight at 4 °C or for 2 h at room temperature, followed by incubation with HRP-conjugated secondary antibodies for 1 h. Protein bands were detected using an enhanced chemiluminescence (ECL) system (Abbkine, California, USA; CAT# BMU102). The use of antibodies is shown in Table 3.

2.7. RNA extraction and quantitative real-time PCR (RT-qPCR)

Total RNA (1 μ g) was extracted using TRIzol reagent (Invitrogen, Carlsbad, California, USA, CAT#10296010CN) and reverse-transcribed into cDNA with random primer in a 20 μ L reaction system. Subsequently, 2 μ L of synthesized cDNA was used for qPCR, which was performed using the ChamQ Universal SYBR qPCR Master Mix instructions (Vazyme, Nanjing, Jiangsu, China, CAT# Q711-02) on a MyiQ Single Color Real-time PCR Detection System (Bio-Rad Laboratories, Hercules, California, USA). Data analysis was performed using the $2^{-\Delta\Delta C_t}$ relative quantitative method in Microsoft Excel. The qPCR primers used in this study are listed in Table 4.

2.8. Cell proliferation assay

DSCs (1×10^4 cells/well) were seeded in a 96-well plate and cultured for 24, 48 and 72 h. Following the respective incubation periods, 10 μ L of Cell Counting Kit-8 (CCK-8) reagent (Vazyme, CAT# A311-02-AA) was added to each well, and the cells were incubated at 37 °C for 1 h. The optical density (OD) at 450 nm was then measured using a microplate reader.

Table 4
qPCR primer sequences.

Gene	Forward Primers (5'-3')	Reverse Primer (5'-3')
FABP5	AGGAGTGGGAATAGCTTTGCG	GCTGAACCAATGCACCATCT
BAX	CCCGAGAGGTCTTTTCCGAG	CCAGCCCATGATGGTTCTGAT
BCL2	GGTGGGGTCATGTGTGTGG	CGGTTCAGGTACTCAGTCATCC
MRPL17	TCGACTATGGGAAGCTGGGA	AGCATTCTTGTGTAGCCCC
MT-ND2	AAACCCCTCGTTCACAGAAGC	GGATTATGGATGCGGTTGCT
MT-ND4	GATTTAGCGGGTGATGCCT	GCTTCAGGGGTTTGATGA
MT-ND4L	TCGCTCACACCTCATATCCTC	AGGCGGCAAGACTAGTATGG
MT-ND5	GCAGCCATTCAAGCAATCCTA	AGGCGAGGATGAAACCGATA
CYTB	TCGGCATTATCCTCCTGCTT	CTCACGGGAGGACATAGCCTCT
MT-CO1	CCCCGCATAAACAACATAAGC	CAGATGCGAGCAGGAGTAGGA
MT-CO2	GCTGTCCCCACATTAGGCTT	CGATGGGCATGAACTGTGG
MT-CO3	AGCCTTTTACCACTCCAGCC	GATTTAGCGGGGTGATGCCT
ATP6	GCCGCAGTACTGATCATTCTATTTC	TCGGTTGTTGATGAGATATTTGA
MMP2	CTTCCAGGGCACATCCTAT	CCTTCTGAGTTCACACAA
MMP9	TCCCTGGAGACCTGAGAACC	GCCACCCGAGTGTAACCAT
CXCL11	GAGTGTGAAGGCATGGCTA	AGGGCCTATGCAAAGACAGC
CXCR3	TGGTCCTGAGGGGTCC	TCCTATAACTGTCCCGCCA
18S rRNA	CGGCTACCACATCCAAGGAA	CTGGAATTACCGCGGCT

2.9. TUNEL assay

The TUNEL assay was performed using the One Step TUNEL Apoptosis Assay Kit (Beyotime, Shanghai, China, CAT# C1089) according to the manufacturer's instructions. Briefly, DSCs were washed with PBS and then fixed with 4 % PFA for 30 min. After an additional PBS wash, the cells were permeabilized with 0.1 % (v/v) Triton X-100/PBS for 15 min. Following two more PBS washes, the cells were incubated with the TUNEL assay solution for an 1 h at 37 °C in the dark. After three final PBS washes, the cells were mounted using a DAPI-containing mounting medium and observed under a fluorescence microscope (Leica DMI8).

2.10. Flow cytometry assay

The apoptosis of treated DSCs was assessed using the Annexin V-Alexa Fluor 647/PI Apoptosis Kit (FcMACS, Nanjing, Jiangsu, China, CAT# FMSAV647-100) according to the manufacturer's instructions. Flow cytometry was performed on a CytoFLEX flow cytometer (Beckman Coulter, Pasadena, California, USA), and data analysis was conducted using CytExpert 2.3 software (Beckman Coulter). Gating was performed using forward scatter (FSC) and side scatter (SSC) parameters.

2.11. Mitochondrial membrane potential (MMP) measurement

MMP was assessed using the JC-1 staining method with the MMP Assay Kit (Beyotime; CAT# C2005) following the manufacturer's protocol. Briefly, DSCs were washed with PBS and incubated with the JC-1 staining working solution for 20 min at 37 °C in the dark. After two additional PBS washes, the cells were mounted using a DAPI-containing mounting medium and observed under a fluorescence microscope (Leica DMI8).

2.12. Cellular ROS analysis

Cellular ROS levels were detected using the Mitochondrial Superoxide Assay Kit with MitoSOX Red (Beyotime; CAT# S0061S) according to the manufacturer's instructions. Briefly, DSCs were washed with PBS and incubated with the MitoSOX Red staining working solution for 15 min at 37 °C in the dark. Following two additional PBS washes, the cells were mounted using a DAPI-containing mounting medium and observed under a fluorescence microscope (Leica DMI8).

2.13. ATP content assay

ATP levels in DSCs were measured using an ATP Assay Kit (Beyotime;

CAT# S0026) following the manufacturer's instructions. Briefly, DSCs were lysed with the provided lysis buffer, and the lysates were centrifuged to collect the cell supernatant (CS). The CS was then mixed with the ATP detection working solution in a 96-well plate. ATP content was quantified using a GloMax 96 Microplate Luminometer (Promega, Madison, Wisconsin, USA).

2.14. RNA sequencing (RNA-seq)

DSCs were transfected with FABP5-targeting siRNA or negative control siRNA for 24 h before being harvested for total RNA isolation. A total of 2 µg RNA from each group was submitted to LC-BIO Technologies Co., Ltd. (Hangzhou, Zhejiang, China) for RNA-seq analysis.

2.15. Enzyme-linked immunosorbent assay (ELISA)

The CS from DSCs was collected and centrifuged at 1,000 rpm for 15 min to remove cell debris. The concentration of CXCL11 in the CS was measured using a human CXCL11 ELISA kit (Boster, Beijing, China; CAT# EK0737) following the manufacturer's instructions.

2.16. Wound healing migration assay

HTR-8/Svneo cells were seeded into 6-well plates and grown until they reached 80–90 % confluence. Wounds were created using a 200 µL pipette tip to generate scratches in the cell monolayer. The cells were then cultured in RPMI 1640 complete medium supplemented with 20 ng/ml recombinant human CXCL11 protein (Sino Biological, Beijing, China; CAT# 10876-HNAE) after transfection with CXCR3-targeting siRNA, or CS from DSCs transfected with FABP5-targeting, MRPL17-targeting, or NC siRNAs. The cultures were incubated at 37 °C in a 5 % CO₂ atmosphere for 12 h. Cell migration was monitored by capturing images using an inverted light microscope (Leica DMI1). The migration area was quantified using Image J software.

2.17. Transwell invasion assay

HTR-8/Svneo cells, at a concentration of 1×10^5 cells/mL, were cultured in 200 µL of FBS-free medium and seeded into chamber inserts pre-coated with Matrigel (BD Biosciences, Franklin Lakes, New Jersey, USA; CAT# 356234). The lower chamber contained RPMI 1640 complete medium supplemented with 50 ng/ml recombinant human CXCL11 protein after transfection with CXCR3-targeting siRNA, or CS from primary DSCs from NP donors transfected with FABP5-targeting, MRPL17-targeting, or NC siRNAs. After 24 h of incubation at 37 °C in a 5 % CO₂ atmosphere, the cells were fixed with 4 % PFA at room

temperature for 10 min and stained with 0.5 % crystal violet (Beyotime; CAT# C0121) for 20 min. Images of the invading cells were captured using an inverted light microscope (Leica DMi1), and the number of invading cells was quantified using Image J software.

2.18. Statistical analysis

All data are expressed as the mean \pm SEM, and all experiments were performed in triplicate. Statistical analyses were conducted using GraphPad Prism 9 software, with a significance level of $P < 0.05$ for two-sided tests. An unpaired student's t -test was used to evaluate differences

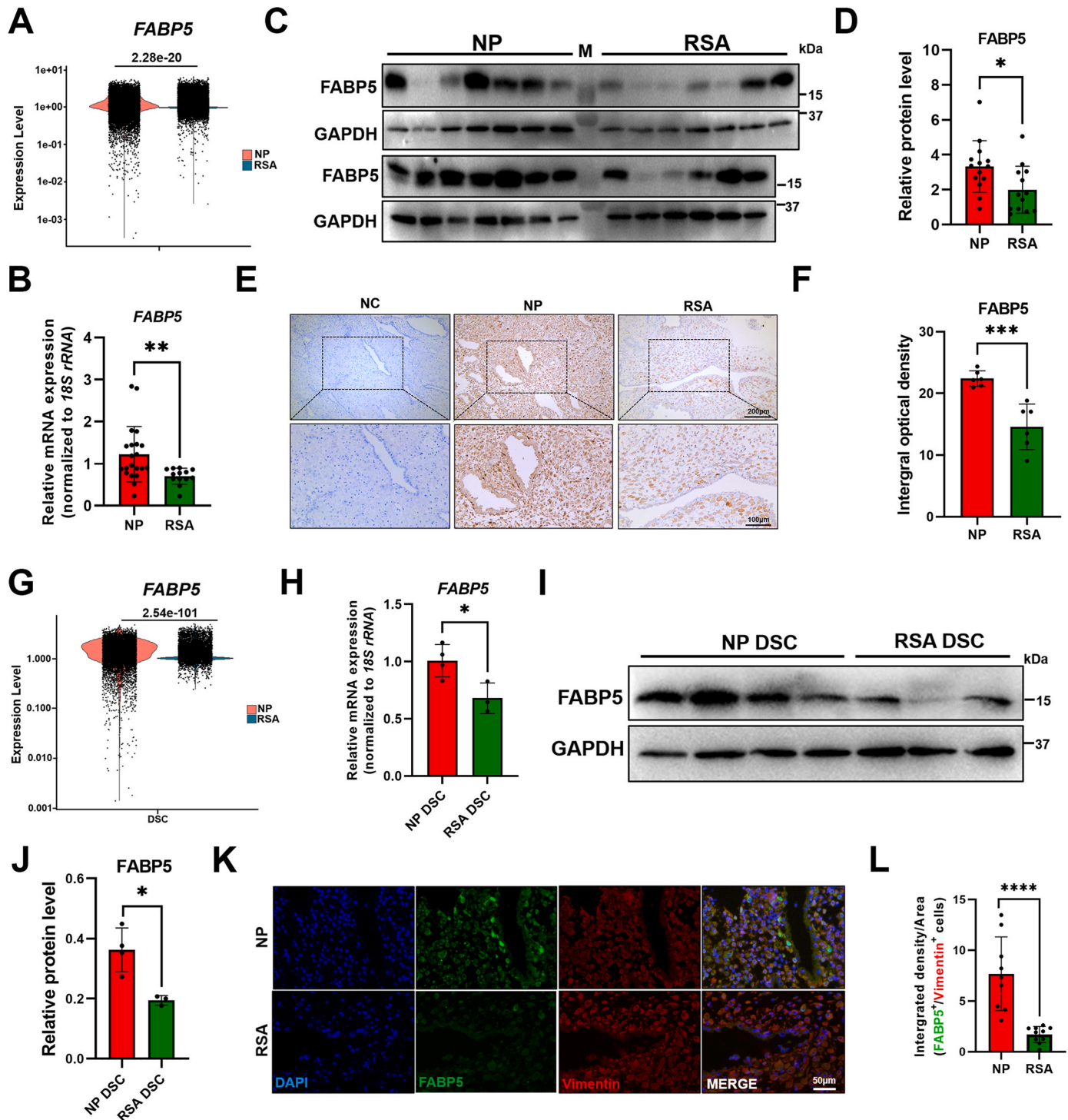


Fig. 1. Aberrant downregulation of *FABP5* in RSA decidual tissues and DSCs. (A) scRNA-seq analysis of *FABP5* expression in decidual tissues from RSA patients and normal pregnancy (NP) controls, as visualized using the ggplot2 package in R. (B) RT-qPCR, (C, D) Western blot, and (E, F) immunohistochemistry analyses of *FABP5* expression in RSA decidual tissues compared to NP controls (scale bars: 200 μ m and 100 μ m). (G) scRNA-seq analysis of *FABP5* expression in DSCs isolated from RSA donors compared to NP controls, as visualized using the ggplot2 package in R. (H) RT-qPCR and (I, J) Western blot analyses of *FABP5* expression in primary DSCs derived from NP and RSA donors. (K, L) Immunofluorescence staining for *FABP5* (green) and Vimentin (red), with nuclear counterstaining using DAPI (blue) in decidual tissues (scale bar: 50 μ m). Statistical significance: * $P < 0.05$, ** $P < 0.01$, *** $P < 0.001$, **** $P < 0.0001$.

between two groups, while two-way analysis of variance (ANOVA) followed by Tukey's post hoc test was applied for comparisons among multiple groups.

3. Results

3.1. The downregulation of FABP5 in RSA DSCs was accompanied by elevated levels of oxidative stress and apoptotic signals

Mounting evidence implicates DSC apoptosis and mitochondrial dysfunction as key contributors to RSA. To test this hypothesis, we collected decidual tissues from both NP and RSA donors to evaluate apoptosis in DSCs. Our results showed a marked increase in Cleaved-Caspase 3 levels in RSA decidual tissues compared to NP tissues (Supplementary Fig. 1A and B). Additionally, Western blot analysis of isolated DSCs revealed a significant upregulation of pro-apoptotic proteins, such as BAX, Cytochrome C (CYTC), and Cleaved-Caspase 3 alongside a downregulation of the anti-apoptotic protein BCL2 in decidual tissues from RSA donors (Supplementary Fig. 1C and D). Moreover, MitoSOX Red and JC-1 staining revealed heightened oxidative stress (Supplementary Fig. 1E and F) and a significant reduction in MMP in DSCs from RSA donors (Supplementary Fig. 1G and H). These findings suggest that oxidative stress-induced apoptosis and mitochondrial damage in DSCs may play a critical role in the pathogenesis of spontaneous abortion.

To characterize FABP5 expression patterns in RSA, we first interrogated publicly available single-cell RNA sequencing (scRNA-seq) data derived from decidual tissues of NP and RSA donors [9]. Bioinformatic analysis demonstrated a consistent and statistically significant downregulation of FABP5 in both bulk decidual tissues and DSCs from RSA donors (Fig. 1A–G). To experimentally validate these observations, we employed a multi-modal approach to systematically evaluate FABP5 expression. qPCR and immunohistochemical analyses corroborated the bioinformatic findings, revealing significantly reduced FABP5 expression in RSA-derived decidual tissues (Fig. 1B–F). To further substantiate these results at the cellular level, we isolated primary DSCs from NP and RSA donors. Comparative analysis confirmed diminished FABP5 expression in RSA-derived DSCs relative to NP controls (Fig. 1H–J). This cell type-specific reduction was further validated through dual immunofluorescence staining, which revealed markedly decreased co-localization of Vimentin and FABP5 in RSA decidual tissues compared to NP samples (Fig. 1K and L).

As previously established, oxidative stress can dysregulate FABP5 expression. To explore this relationship mechanistically, we exposed primary DSCs from NP donors (Hereinafter collectively referred to as primary DSCs) to TBHP to induce oxidative stress *in vitro*. TBHP treatment significantly increased intracellular ROS while reducing MMP (Supplementary Fig. 2A–D), confirming successful oxidative stress induction. Notably, TBHP-challenged DSCs exhibited coordinated downregulation of FABP5 expression, accompanied by a pronounced shift in apoptotic regulators, characterized by upregulation of pro-apoptotic factors (BAX, CYTC, and Cleaved-Caspase 3) and concurrent downregulation of the anti-apoptotic protein BCL2 (Supplementary Fig. 2E–G). Consistent with these molecular changes, we observed robust apoptotic signatures in TBHP-treated primary DSCs (Supplementary Fig. 2F–I). These findings demonstrate that oxidative stress downregulates FABP5 in DSCs, triggering mitochondrial dysfunction and apoptosis. This oxidative stress-FABP5-apoptosis axis may underlie RSA pathogenesis.

3.2. Knockdown of FABP5 exacerbates apoptosis and mitochondrial damage in DSCs

Given that FABP5 deficiency has been demonstrated to inhibit cell proliferation and promotes apoptosis [18,19], we hypothesized that FABP5 downregulation might disrupt the survival regulation of DSCs in

RSA. To examine this possibility, we performed FABP5 knockdown in DSCs using FABP5-targeting siRNA under *in-vitro* conditions. Our results showed that FABP5 silencing markedly elevated the mRNA expression of the pro-apoptotic gene BAX while reducing that of the anti-apoptotic gene BCL2 in DSCs (Fig. 2A). Correspondingly, at the protein level, FABP5 knockdown led to increased expression of pro-apoptotic markers including BAX, CYTC, and Cleaved-Caspase 3, accompanied by decreased levels of the anti-apoptotic protein BCL2 (Fig. 2B and C). This apoptotic effect was further validated by TUNEL staining, which displayed significantly enhanced apoptotic signals in primary DSCs following FABP5 knockdown (Fig. 2D and E). Flow cytometric analysis provided additional evidence, revealing substantial increases in both early and late apoptotic cell populations in primary DSCs with FABP5 knockdown (Fig. 2F and G). Furthermore, we detected a notable reduction in Ki67-positive cells, and CCK8 proliferation assays demonstrated significantly diminished proliferative capacity in primary DSCs 48 h after FABP5 knockdown (Supplementary Fig. 3A–C). These collective findings strongly suggest that FABP5 downregulation induces survival dysregulation in DSCs.

Building upon previous studies demonstrating that FABP5 deficiency induces severe mitochondrial damage [21,22], and given the established association between mitochondrial dysfunction and apoptosis, we proposed that FABP5 downregulation might promote DSC apoptosis through mitochondrial impairment. Supporting this hypothesis, our experiments revealed that FABP5 knockdown in primary DSCs led to a significant reduction in MMP (Fig. 2H and I), indicative of substantial mitochondrial injury. We further observed that FABP5 silencing caused distinct mitochondrial morphological alterations, including fragmentation and loss of structural continuity (Fig. 2J), accompanied by decreased ATP generation (Fig. 2K). In summary, these findings collectively demonstrate that FABP5 deficiency induces mitochondrial damage in DSCs, ultimately triggering apoptotic cell death.

3.3. Downregulation of FABP5 led to decreased expression of MRPL17 in RSA DSCs

To further investigate the molecular mechanisms by which FABP5 downregulation induces mitochondrial damage and apoptosis in DSCs, we performed RNA-seq analysis comparing DSCs transfected with FABP5-targeting siRNA versus NC siRNA. Bioinformatic analysis identified mitochondrial ribosomal protein L17 (MRPL17) as significantly enriched in the “mitochondrion” GO term (Fig. 3A). Both volcano map and heat map analyses demonstrated marked downregulation of MRPL17 following FABP5 knockdown (Fig. 3B and C).

Subsequent validation experiments confirmed this regulatory relationship at both transcriptional and translational levels. FABP5 silencing significantly reduced MRPL17 expression, with immunofluorescence revealing co-localization of these proteins in DSCs (Fig. 3D–H). To assess the clinical relevance of these findings, we examined MRPL17 expression patterns in clinical samples. Analysis of the scRNA-seq data [9] revealed significantly decreased MRPL17 expression in both bulk decidual tissues and DSC populations from RSA donors compared to NP controls (Fig. 3I–N). These observations were further validated at both mRNA and protein levels (Fig. 3J–L, N, O–Q). Notably, correlation analysis revealed a significant positive association between FABP5 and MRPL17 expression in decidual tissues (Fig. 3K). These findings collectively demonstrate that MRPL17 serves as a downstream effector of FABP5-mediated mitochondrial regulation in DSCs, providing novel mechanistic insights into the pathogenesis of RSA.

3.4. FABP5 knockdown induced mitochondrial damage and apoptosis in DSCs by suppressing MRPL17 expression

Given the limited existing research on MRPL17, we sought to determine whether its downregulation directly contributes to mitochondrial dysfunction and apoptosis in FABP5-deficient DSCs. Efficient

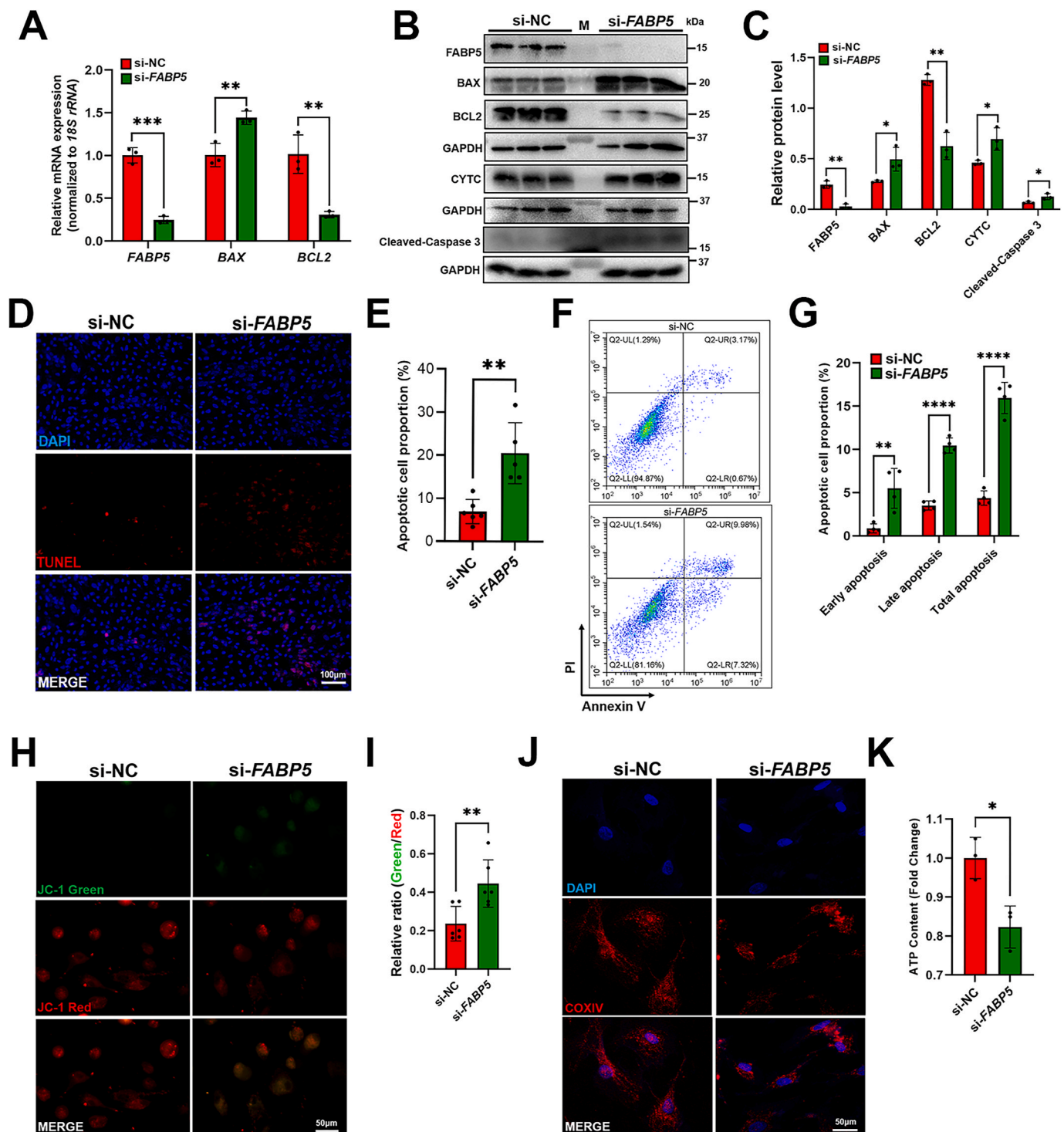


Fig. 2. Knock-down of FABP5 induces survival disorders and mitochondrial damage in DSCs. (A) RT-qPCR and (B, C) Western blot analyses assessing expression levels of FABP5, BAX, CYTC, Cleaved-Caspase 3, and BCL2 in primary DSCs following transfection with FABP5-targeting or NC siRNAs. (D, E) TUNEL staining for detection of DNA fragmentation in siRNA-transfected DSCs, with nuclear counterstaining using DAPI (scale bar = 100 μm). (F, G) Flow cytometry evaluation of apoptosis rates in FABP5-knockdown and control DSCs. (H, I) JC-1 staining reveals MMP in FABP5-knockdown and control DSCs (scale bar = 50 μm). (J) Immunofluorescence staining of COXIV for evaluation of mitochondrial morphology, with DAPI nuclear counterstaining (scale bar = 50 μm). (K) Measurement of intracellular ATP levels in FABP5-knockdown and control DSCs. Statistical significance: * $P < 0.05$, ** $P < 0.01$, **** $P < 0.0001$.

MRPL17 knockdown was confirmed by RT-qPCR and western blotting (Fig. 4A and B). Similarly to FABP5 deficiency, MRPL17-deficient DSCs exhibited pronounced apoptotic features, including upregulated proapoptotic markers (BAX, CYTC, Cleaved-Caspase 3) and down-regulated BCL2 (Fig. 4A–C). These findings were corroborated by increased apoptosis in TUNEL assays and flow cytometry (Fig. 4D–G),

along with impaired proliferation (Supplementary Fig. S3D–F). MRPL17 knockdown also induced mitochondrial dysfunction, characterized by reduced MMP (Fig. 4H and I), abnormal mitochondrial morphology (Fig. 4J), and decreased ATP production (Fig. 4K). These results suggest that MRPL17, as a downstream molecule of FABP5, play a crucial role in regulating DSC survival and mitochondrial function.

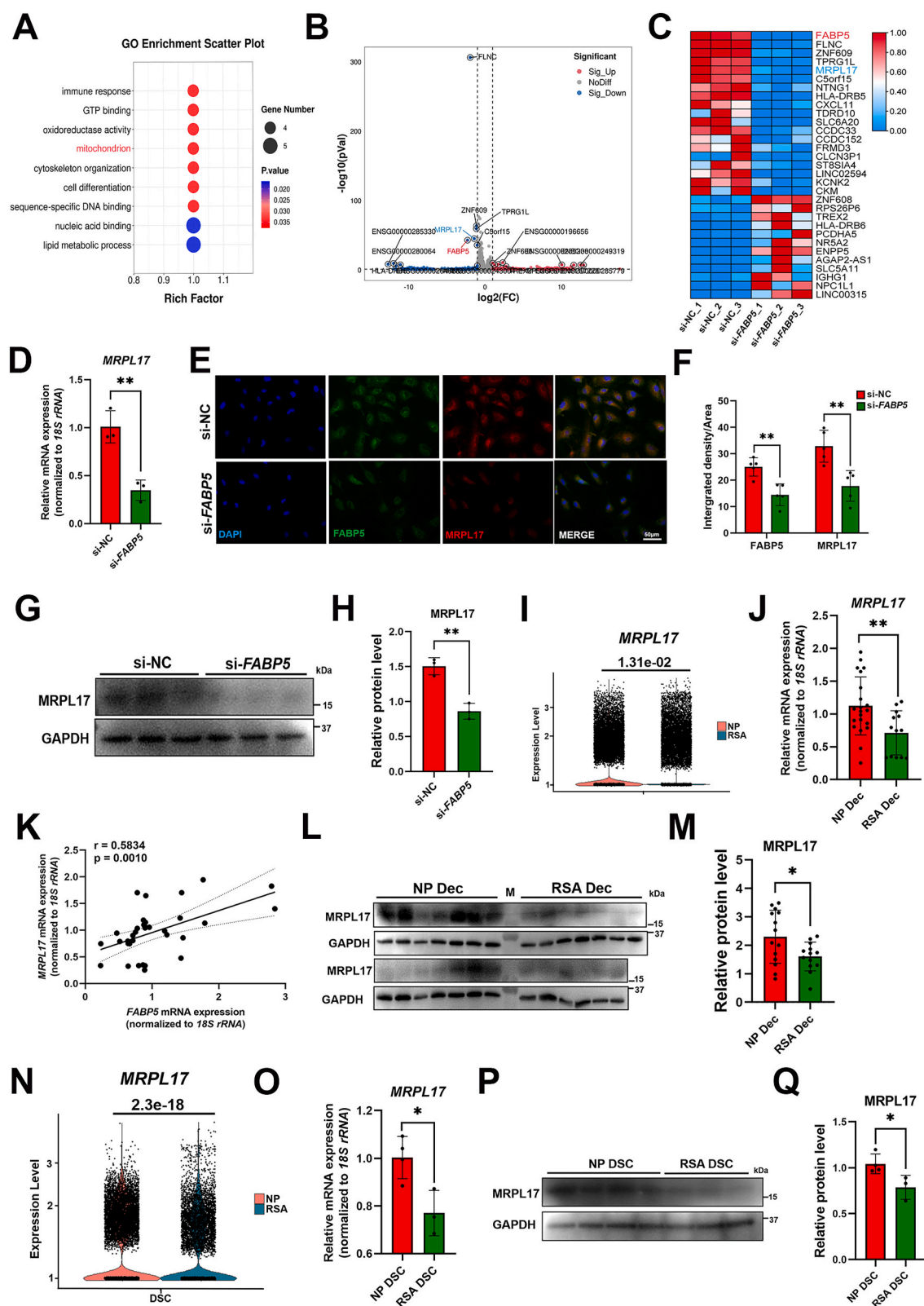


Fig. 3. FABP5 directed the downstream molecule MRPL17, which is downregulated in RSA decidual tissues and DSCs. (A) GO analysis of the differentially expressed genes (DEGs) identified by RNA-seq following FABP5 knockdown in primary DSCs. (B) Volcano plot from RNA-seq data highlighting DEGs, including FABP5 and MRPL17. (C) Heatmap representation of DEGs from RNA-seq analysis, featuring FABP5 and MRPL17. (D) RT-qPCR, (E, F) Immunofluorescence colocalization, and (G, H) Western blot analyses of MRPL17 protein levels following FABP5 knockdown (Scale bar = 100 μm). (I) scRNA-seq analysis comparing MRPL17 expression in RSA and NP decidual tissues (visualized with ggplot2 in R). (J) Measurement of MRPL17 mRNA levels in RSA versus NP decidual tissues. (K) Pearson correlation analysis of FABP5 and MRPL17 mRNA expression. (L, M) Western blot evaluation of MRPL17 protein expression in RSA and NP decidual tissues. (N) scRNA-seq analysis of MRPL17 expression in DSCs isolated from RSA and NP cases (visualized with ggplot2 in R). (O) RT-qPCR and (P, Q) Western blot assessment of MRPL17 mRNA and protein in primary DSCs derived from NP and RSA decidual tissues. Statistical significance: * $P < 0.05$, ** $P < 0.01$.

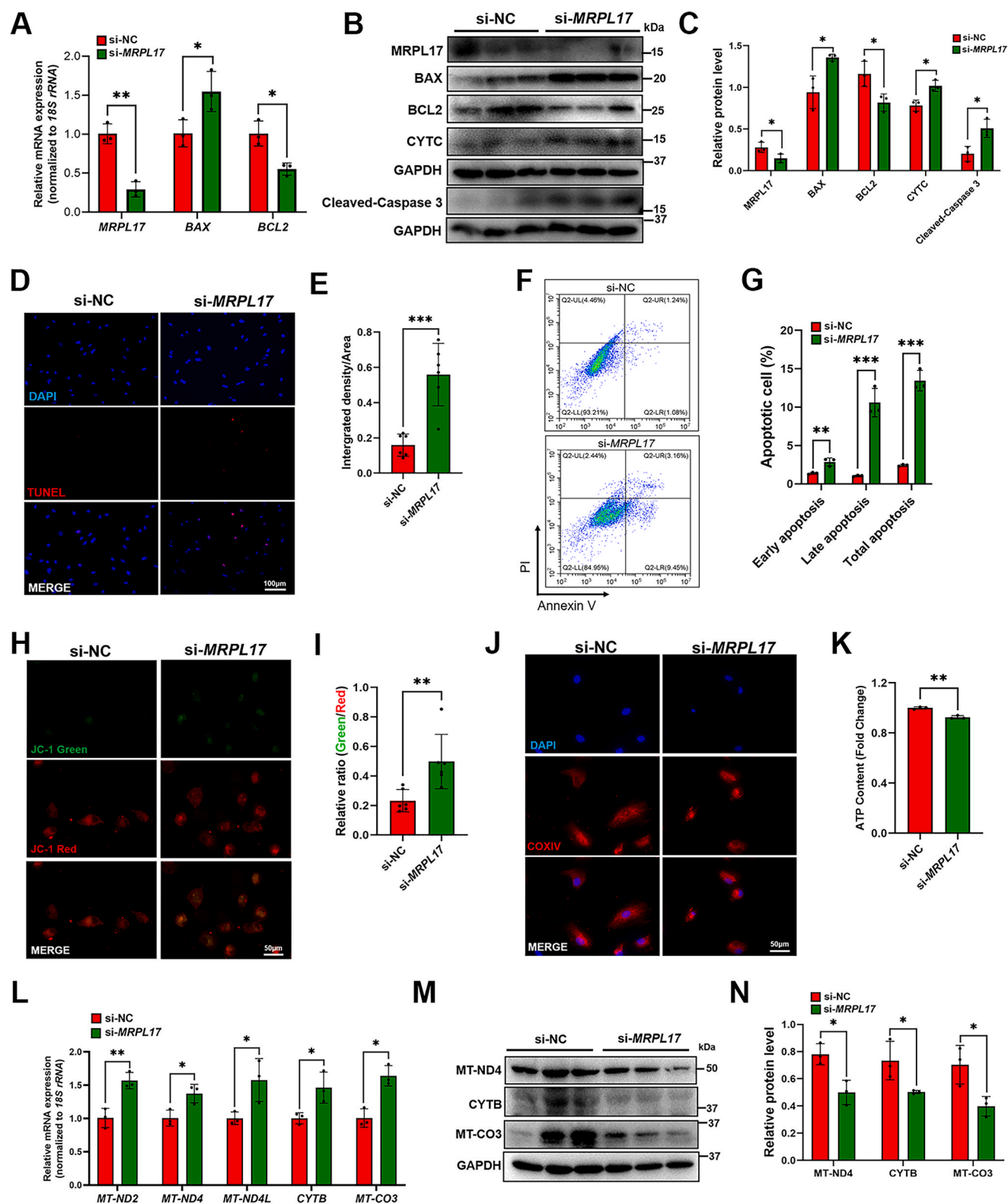


Fig. 4. MRPL17 knockdown impaired DSC survival and mitochondrial function. (A) RT-qPCR and (B, C) Western blot analyses of MRPL17, BAX, CYTC, Cleaved-Caspase 3, and BCL2 expression in primary DSCs transfected with MRPL17-targeting or NC siRNAs. (D, E) TUNEL staining for DNA fragmentation assessment in siRNA-transfected DSCs, with DAPI nuclear counterstaining (scale bar = 100 μm). (F, G) Flow cytometric evaluation of apoptosis rates in MRPL17-knockdown and control DSCs. (H, I) JC-1 staining for MMP analysis (scale bar = 50 μm). (J) Immunofluorescence staining of COXIV for mitochondrial morphology evaluation, with DAPI nuclear counterstaining (scale bar = 50 μm). (K) Measurement of intracellular ATP levels in experimental and control groups. (L) RT-qPCR and (M, N) Western blot analyses of mitochondrial gene expression (MT-ND2, MT-ND4, MT-ND4L, CYTB, and MT-CO3) following MRPL17 knockdown. Statistical significance: * $P < 0.05$, ** $P < 0.01$, *** $P < 0.001$.

As a mitochondrial ribosomal protein component, MRPL17 participates in translating genes encoded by mitochondrial DNA (mtDNA). Our RNA-seq analysis of FABP5-knockdown DSCs revealed that dysregulation of 4 out of the 13 mitochondrial genes (MT-ND1, MT-ND2, MT-ND3, MT-ND4, MT-ND4L, MT-ND5, MT-ND6, CYTB, MT-CO1, MT-CO2, MT-CO3, ATP6, and ATP8) encoding subunit proteins of the respiratory chain complex in oxidative phosphorylation (OXPHOS) system (Supplementary Fig. 4A). Intriguingly, while MRPL17 or FABP5 knockdown increased mRNA levels of MT-ND2, MT-ND4, MT-ND4L, CYTB, and MT-CO3 (Supplementary Fig. 4B; Fig. 4L), their protein products were significantly reduced (Supplementary Fig. 4C and D; Fig. 4M and N), suggesting translational impairment.

To establish causality, we performed rescue experiments by over-expressing Flag-tagged MRPL17 in FABP5-deficient DSCs. MRPL17

restoration significantly attenuated apoptosis (reduced BAX, increased BCL2; Fig. 5A) and decreased apoptotic cell populations (Fig. 5B–E). Proliferation capacity (Supplementary Fig. 3G–I) and mitochondrial parameters (MMP, ATP production, and morphology; Fig. 5F–I) were all partially rescued. Notably, MRPL17 overexpression normalized the aberrant mRNA elevation of MT-ND2, MT-ND4, MT-ND4L, CYTB, and MT-CO3 in FABP5-deficient DSCs (Fig. 5J). In summary, our findings strongly suggest that FABP5 depletion triggered DSC apoptosis and mitochondrial dysfunction through MRPL17's regulation of the synthesis of respiratory chain complex subunit proteins in OXPHOS system.

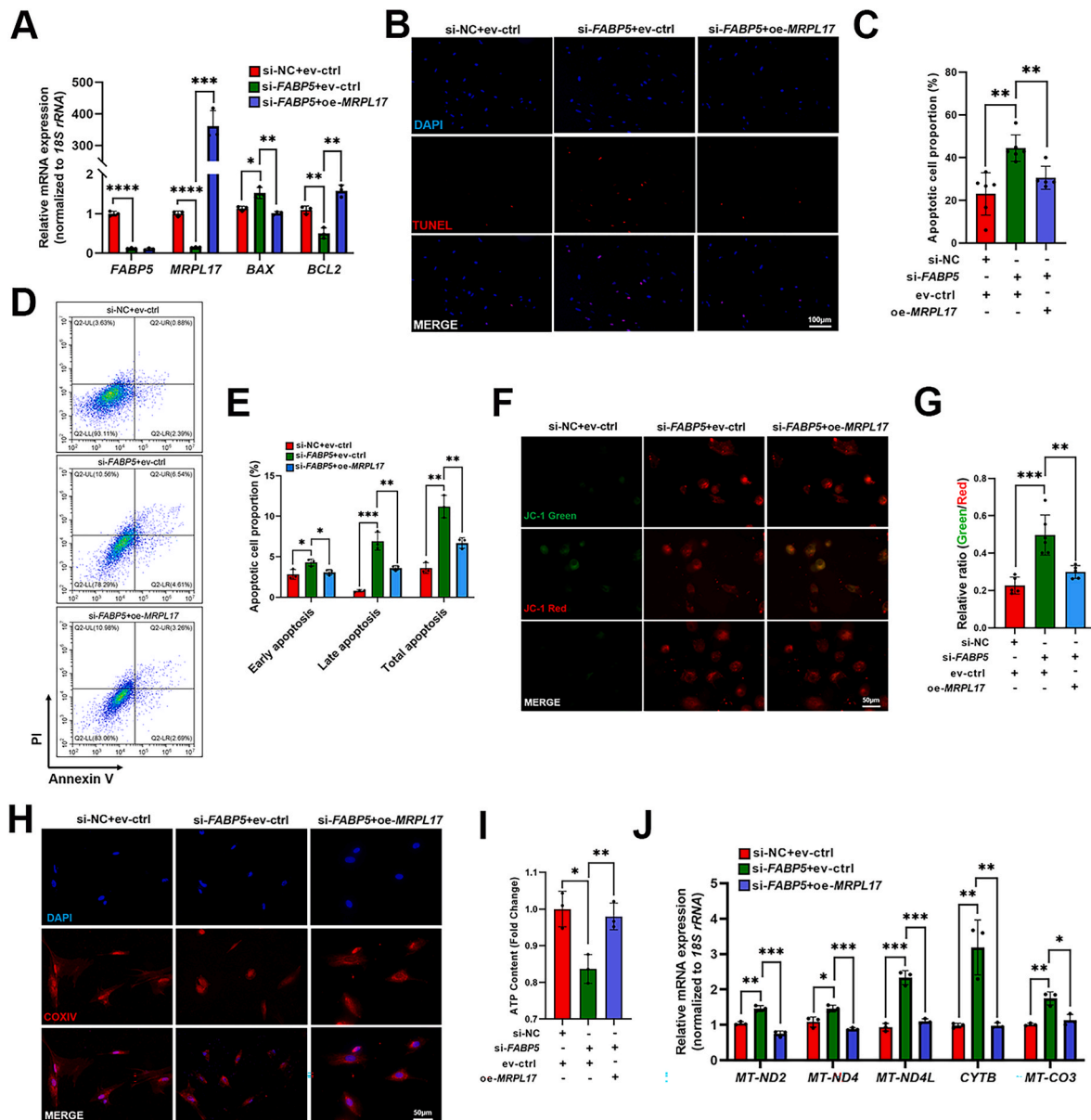


Fig. 5. MRPL17 overexpression rescues DSC survival and mitochondrial function disrupted by FABP5 knockdown. (A) RT-qPCR analysis of MRPL17, BAX, and BCL2 expression in primary DSCs following co-transfection with FABP5-targeting siRNA and Flag-tagged MRPL17 plasmid. (ev-ctrl: empty vector control; oe-MRPL17: MRPL17 overexpression) (B, C) TUNEL staining for DNA fragmentation assessment in experimental groups, with DAPI nuclear counterstaining (scale bar = 100 μm). (D, E) Flow cytometric evaluation of apoptosis rates in co-transfected DSCs. (F, G) JC-1 staining for MMP analysis (scale bar = 50 μm). (H) Immunofluorescence staining of COXIV for mitochondrial morphology evaluation, with DAPI nuclear counterstaining (scale bar = 50 μm). (I) Measurement of intracellular ATP levels in experimental and control groups. (J) RT-qPCR analysis of respiratory chain complex subunit gene expression in the OXPHOS system. Statistical significance: * $P < 0.05$, ** $P < 0.01$, *** $P < 0.001$, **** $P < 0.0001$.

3.5. FABP5 regulated trophoblast cell migration and invasion by modulating CXCL11 secretion in DSCs

The decidua plays a critical role in pregnancy by establishing a cytokine/chemokine microenvironment that guides extravillous trophoblast invasion while simultaneously acting as a physical barrier to prevent excessive trophoblast penetration [23–28]. Previous studies have demonstrated that impaired communication between DSCs and trophoblasts contributes to RSA [29–31]. To investigate whether FABP5 deficiency in DSCs affects trophoblast behavior, we collected the CS from FABP5-deficient DSCs and used it to treat HTR-8/Svneo cells. Functional assays revealed that CS from FABP5-deficient DSCs significantly inhibited HTR-8/Svneo cell migration and invasion, as demonstrated by both wound healing and transwell assays (Fig. 6A–D). This impaired motility was accompanied by reduced expression of matrix metalloproteinases (MMPs) 2 and 9, crucial for extracellular matrix remodeling during trophoblast invasion (Fig. 6E–G). Similar results were observed when using CS from MRPL17-deficient DSCs (Supplementary Fig. 5), suggesting that both FABP5 and its downstream effector MRPL17 regulate DSC secretory properties that influence trophoblast function.

To elucidate the molecular mechanisms underlying these observations, we performed Kyoto Encyclopedia of Genes and Genomes (KEGG) pathway analysis of RNA-seq data from FABP5-knockdown DSCs, which revealed significant alterations in chemokine signaling pathways (Fig. 7A and B). Among the affected chemokines, CXCL11 showed particularly pronounced downregulation following FABP5 knockdown (Fig. 7C–G). This finding was validated at both mRNA and protein levels, with parallel results observed in MRPL17-deficient DSCs (Supplementary Fig. 6A–D). Given that CXCL11 signals through its receptor CXCR3 to regulate cell migration and invasion [32–34], we examined CXCR3 expression in HTR-8/Svneo cells treated with CS from FABP5- or MRPL17-deficient DSCs. In both cases, CXCR3 expression was significantly suppressed (Fig. 7H–J; Supplementary Fig. 6E–G), providing a potential mechanism for the observed impairment in trophoblast motility. Rescue experiments further supported this mechanistic pathway. Overexpression of MRPL17 in FABP5-deficient DSCs

restored CXCL11 expression (Supplementary Fig. 7A and B). Consequently, when HTR-8/Svneo cells were treated with CS from these rescued DSCs, they showed recovered expression of CXCR3, MMP2, and MMP9, along with improved migratory and invasive capacities (Supplementary Fig. 7C–I).

To further elucidate the functional contribution of the CXCL11/CXCR3 axis to trophoblast migration and invasion, CXCR3 expression was genetically silenced in HTR8 cells using specific siRNA. This knockdown resulted in significant downregulation of MMP2 expression (Supplementary Fig. 8A and B), along with markedly impaired cellular migration (Supplementary Fig. 8C and D) and invasion capabilities (Supplementary Fig. 8E and F). Importantly, these suppressive effects were significantly attenuated following treatment with recombinant CXCL11 protein (Supplementary Fig. 8A–F). These findings collectively demonstrate that FABP5 regulates trophoblast function through an MRPL17-dependent mechanism that modulates CXCL11 secretion from DSCs. The disruption of this FABP5/MRPL17/CXCL11/CXCR3 signaling axis between DSCs and trophoblasts may represent a key pathogenic mechanism in RSA, providing new insights into the molecular basis of pregnancy complications associated with impaired trophoblast invasion.

4. Discussion

RSA represents a complex pregnancy disorder with diverse etiological factors, among which uterine dysfunction has been increasingly recognized as a significant contributor [1–3,35]. As the predominant cellular component of the decidualized endometrium, DSCs play pivotal roles in orchestrating trophoblast invasion and maintaining pregnancy homeostasis [6,29–31]. Our current findings reveal that oxidative stress-mediated FABP5 downregulation initiates a pathogenic cascade in RSA through multiple mechanisms.

At the cellular level, FABP5 deficiency leads to MRPL17 suppression, which in turn triggers mitochondrial dysfunction through two distinct pathways: activation of the intrinsic apoptotic pathway and impairment of oxidative phosphorylation (OXPHOS) system assembly. The mitochondrial perturbations manifest as disrupted membrane potential, structural abnormalities, and compromised ATP production.

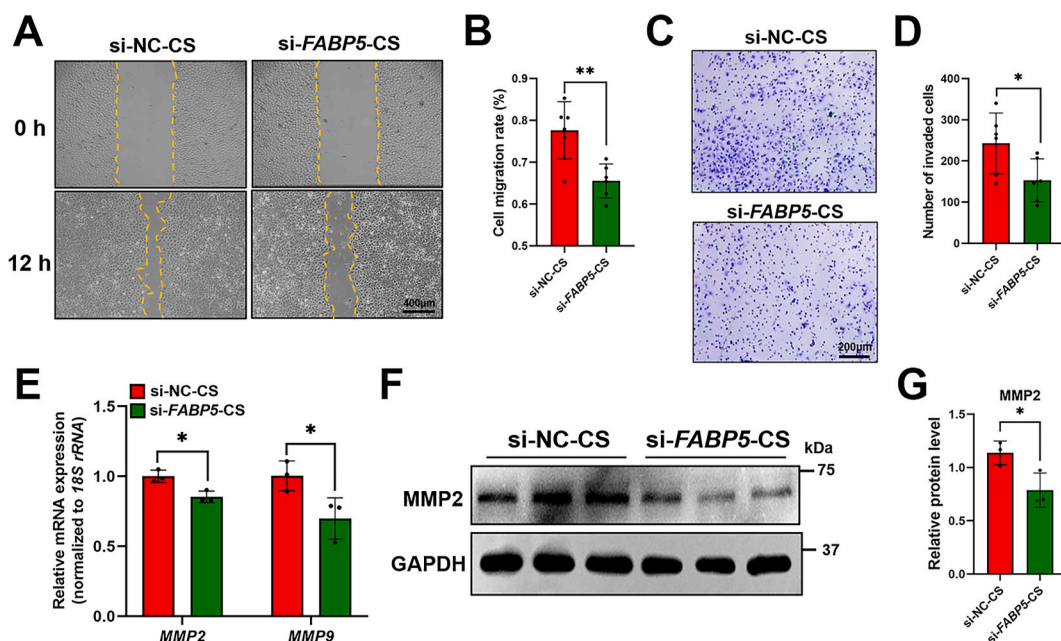


Fig. 6. FABP5-deficient DSC supernatant impairs the migration and invasion of HTR-8/Svneo cells. (A, B) Wound healing assay assessing HTR-8/Svneo cell migration following stimulation with CS from FABP5-knockdown primary DSCs (scale bar = 400 μ m). (C, D) Transwell invasion assay evaluating HTR-8/Svneo cell invasive capacity after treatment with CS from FABP5-deficient DSCs (scale bar = 200 μ m). (E) RT-qPCR and (F, G) Western blot analyses of MMP2 and MMP9 expression in HTR-8/Svneo cells exposed to CS from FABP5-knockdown primary DSCs. Statistical significance: * P < 0.05, ** P < 0.01.

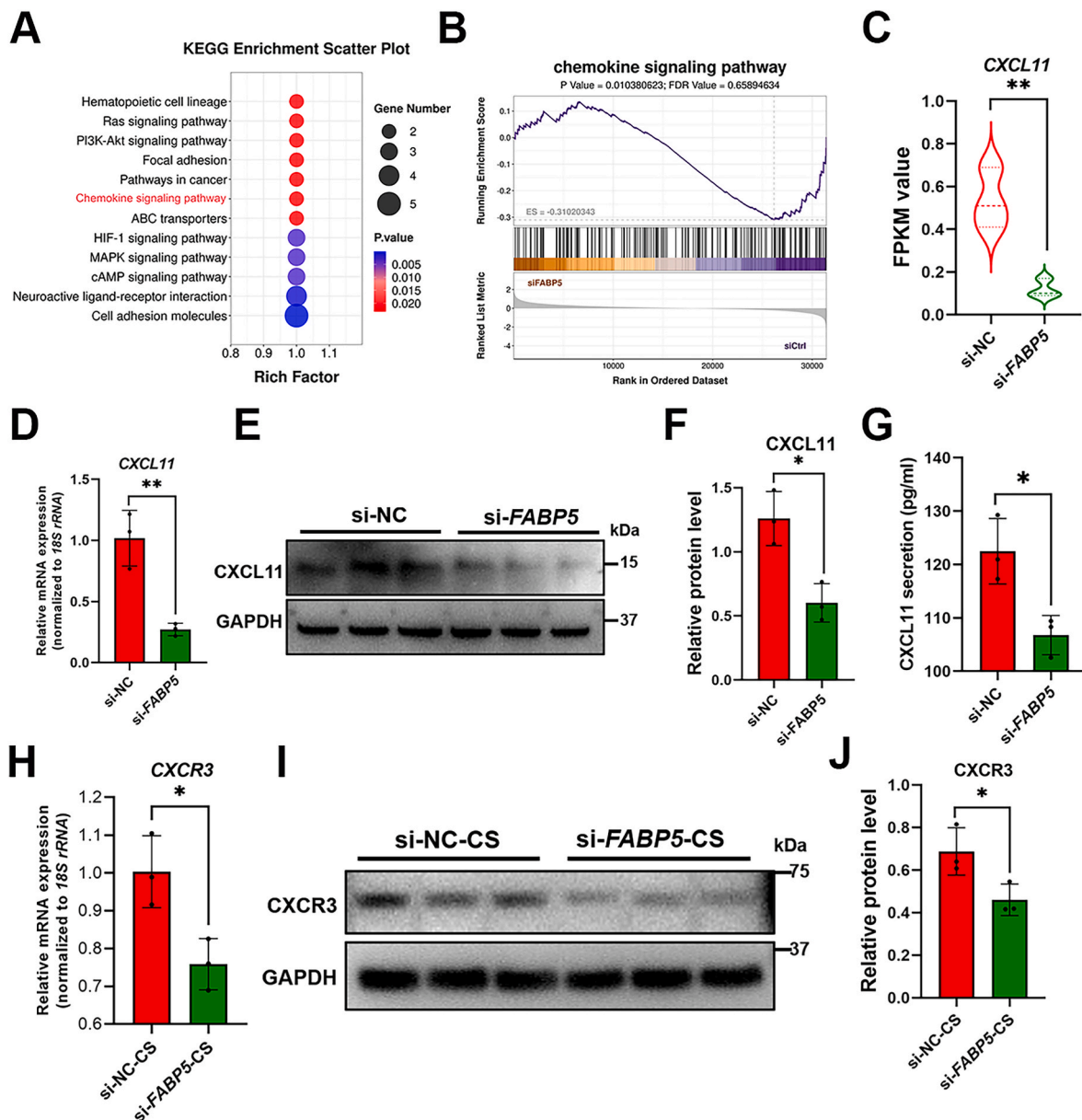


Fig. 7. FABP5 downregulation in DSCs repressed CXCL11/CXCR3 signaling between DSCs and HTR-8/Svneo cells. (A) KEGG pathway analysis of DEGs identified by RNA-seq in FABP5-knockdown primary DSC. (B) Gene Set Enrichment Analysis (GSEA) of chemokine signaling pathways in FABP5-silenced DSCs. (C) FPKM values of CXCL11 expression in control and FABP5-knockdown groups. (D) RT-qPCR, (E, F) Western blot, and (G) ELISA quantification of CXCL11 expression in DSCs transfected with FABP5-targeting or NC siRNAs. (H) RT-qPCR and (I, J) Western blot analyses of CXCR3 expression in HTR-8/Svneo cells treated with CS from FABP5-deficient or control DSCs. Statistical significance: * $P < 0.05$, ** $P < 0.01$.

Simultaneously, we identified that FABP5 downregulation alters the decidual secretome, particularly through reduced CXCL11 secretion, resulting in diminished CXCR3 expression and consequent impairment of trophoblast migratory capacity.

These molecular alterations were consistently observed in clinical RSA specimens, where we documented concurrent downregulation of both FABP5 and MRPL17, accompanied by characteristic mitochondrial damage and elevated apoptotic indices in DSCs. The dual impact on both DSC survival and trophoblast function positions the FABP5/MRPL17 axis as a critical regulatory node in pregnancy maintenance. Our findings provide a mechanistic framework linking oxidative stress to the core pathological features of RSA through this newly identified molecular pathway. The comprehensive nature of these effects-encompassing cell survival, energy metabolism, and paracrine signaling - underscores the central role of DSC homeostasis in pregnancy success and suggests

that therapeutic strategies targeting the FABP5/MRPL17 pathway may hold promise for RSA intervention.

At the maternal-fetal interface, the survival of DSCs is tightly regulated by their crosstalk with immune and trophoblast cell populations, including natural killer (NK) cells [36–38], T cells [39,40], macrophages [41], and placental trophoblasts [29–31]. Dysregulation of DSC homeostasis, particularly excessive apoptosis, disrupts these interactions and is implicated in pregnancy complications such as spontaneous abortion and RSA [42–44]. Here, we demonstrate that DSC apoptosis critically modulates cellular communication at the maternal-fetal interface, with mechanistic relevance to RSA pathogenesis. Specifically, we uncover the FABP5/MRPL17/CXCL11/CXCR3 axis as a novel molecular pathway that orchestrates DSC survival and trophoblast function. This axis mitigates DSC apoptosis and mitochondrial dysfunction while maintaining decidual homeostasis, thereby

promoting successful pregnancy outcomes.

Interestingly, mitochondrial genes including MT-ND4, CYTB, and MT-CO3 exhibit discordant expression patterns at the transcriptional and translational levels following FABP5 or MRPL17 knockdown in DSCs. Our findings indicate that MRPL17, a core component of the mitochondrial ribosomal protein family, orchestrates mitochondrial gene expression and rescues mitochondrial translation deficiency [44]. This aligns with prior studies demonstrating the indispensable roles of other mitochondrial ribosomal proteins (e.g., MRPL12 [45–47], MRPL50 [48], MRPL10 [49], MRPL13 [50]) in facilitating the translation of OXPHOS system subunits. We hypothesize that MRPL17 downregulation—whether mediated by MRPL17-targeting siRNA or FABP5 silencing—compromises the translation of these mitochondrial-encoded subunits. Consequently, unprocessed MT-ND4, CYTB, and MT-CO3 mRNAs accumulate, failing to undergo efficient protein synthesis.

Beyond DSCs, the anti-apoptotic effects of FABP5 have been documented in diverse cellular contexts. In gastric cancer cells, FABP5 knockdown suppresses the Hippo pathway, potentiating apoptosis [19]. Likewise, pharmacological inhibition of FABP5 by SBFI-26 induces apoptosis in prostate cancer cell by attenuating PPAR γ activity, which subsequently activates pro-apoptotic AKT or NF- κ B signaling [51]. In contrast, our work reveals that FABP5 knockdown in DSCs predominantly activates the intrinsic mitochondrial apoptotic pathway, characterized by elevated BAX and CYTC expression coupled with reduced BCL2 levels. This cell type-specific disparity underscores the context-dependent anti-apoptotic mechanisms of FABP5.

Furthermore, FABP5 exhibits dualistic roles in mitochondrial regulation across cell types. In cardiac fibroblasts, FABP5 deficiency exacerbates oxidative stress and mitochondrial dysfunction, aggravating pathological remodeling [21]. Conversely, in human neuroblastoma SHSY5Y cells under oxidative stress, FABP5 overexpression amplifies MMP collapse and cell death-effects rescued by the FABP5 inhibitor HY11-08 [22]. These findings collectively demonstrate that the functional consequences of FABP5 on mitochondrial integrity are highly cell type-contextual, ranging from protective to detrimental.

As noted earlier, DSC-derived cytokines and chemokines are pivotal mediators of cellular crosstalk within the decidua and at the maternal-fetal interface, orchestrating key processes for pregnancy maintenance. Notably, FABP5 emerges as a multifunctional modulator of cytokine/chemokine secretion in secretory cells. Consistent with this role, FABP5 inhibition in human and rat models attenuates osteoarthritis pain by suppressing pro-nociceptive cytokines (IL-6, IL-8) and chemokines (CCL2, CXCL1) [52]. Similarly, genetic ablation of FABP5 in mice disrupts NF- κ B signaling via its interaction with valosin-containing protein (VCP), leading to impaired chemokine secretion in central granulocytes [53]. This regulatory function extends to other fatty acid-binding protein family members. For instance, epidermal fatty acid binding protein (E-FABP) deletion downregulates cytosolic phospholipase A2/peroxisome proliferator-activated receptor β (cPLA2/PPAR β) activity, resulting in reduced secretion of CXCL1 and cyclooxygenase-2 (COX-2) [54]. Conversely, elevated FABP4 expression augments tissue-resident memory T cell survival and activation by enhancing fatty acid metabolism and CXCL10 secretion [55]. In agreement with these observations, our data demonstrate that FABP5 knockdown in DSCs specifically diminishes CXCL11 secretion. Collectively, these findings reinforce the conserved role of FABP5-and related fatty acid-binding proteins-in governing cytokine/chemokine output from secretory cells across physiological and pathological contexts.

While our study elucidates the pathophysiological significance of the FABP5/MRPL17/CXCL11/CXCR3 axis in DSC-trophoblast interactions, several limitations warrant consideration. First, the current findings are primarily derived from *in-vitro* models. Future studies employing conditional knockout mouse models will be essential to validate these mechanisms *in vivo*. Second, while we observed consistent patterns in

both isolated DSCs and decidual tissues, the clinical cohort size was limited due to stringent inclusion criteria and sample availability at our single-center institution. Expanding the sample size through multicenter collaborations would enhance the statistical power and generalizability of our conclusions.

In conclusion, our work identifies aberrantly low FABP5 expression as a key contributor to RSA pathogenesis, driving mitochondrial dysfunction and apoptosis in DSCs while compromising CXCL11-mediated trophoblast support. These findings not only advance our understanding of RSA mechanisms but also highlight the FABP5/MRPL17/CXCL11/CXCR3 axis as a potential therapeutic target. Future translational studies aimed at modulating this pathway could pave the way for novel RSA treatment strategies.

CRediT authorship contribution statement

Dong Li: Writing – review & editing, Writing – original draft, Visualization, Validation, Supervision, Software, Resources, Project administration, Methodology, Investigation, Formal analysis, Data curation, Conceptualization. **Honglei Duan:** Visualization, Validation, Project administration, Methodology, Investigation, Funding acquisition. **Zihan Jiang:** Resources, Project administration. **Chunxiang Zhou:** Resources, Project administration. **Chenrui Cao:** Resources, Project administration. **Mengyao Ni:** Resources, Project administration. **Linlin He:** Resources, Project administration, Methodology. **Xiangyu Zhu:** Validation, Methodology. **Liang Jin:** Resources. **Wei Liu:** Validation, Methodology. **Leilei Gu:** Validation, Methodology. **Huijun Li:** Validation, Methodology. **Dan Liu:** Conceptualization. **Xiaolei Zhao:** Validation, Resources, Investigation. **Guangfeng Zhao:** Supervision, Project administration, Conceptualization. **Jie Li:** Writing – review & editing, Supervision, Funding acquisition, Data curation, Conceptualization.

Ethics approval and consent to participate

Informed consent was obtained from all participants prior to undergoing the induced abortion procedure. The use of human decidual tissues was approved by the Ethics Committee of Nanjing Drum Tower Hospital in accordance with the Declaration of Helsinki on January 11, 2021 (Approval No. 2021-464-02), with written informed contents obtained from all patients.

Availability of data and materials

The RNA-seq datasets for FABP5 knockdown used in this study are available in the NCBI Sequence Read Archive (SRA) under accession number PRJNA1189276 and can be accessed upon request.

Funding

This work was supported by the funding for Clinical Trials from the Affiliated Drum Tower Hospital, Medical School of Nanjing University [grant number 2022-LCYJ-MS-06], and the Special Fund for the Development of Health Science and Technology in Nanjing, China [grant number YKK21096].

Declaration of competing interest

The authors declare no conflicts of interest.

Acknowledgements

We would like to extend our gratitude to Du et al. for generously sharing their scRNA-seq data in public databases. We also sincerely thank LC-BIO Technologies Co., Ltd. for providing RNA-seq services. The schematic diagram of the graphical abstract was drawn by Figdraw.

Appendix A. Supplementary data

Supplementary data to this article can be found online at <https://doi.org/10.1016/j.freeradbiomed.2025.06.003>.

Abbreviations

DSCs	Decidual stromal cells
RSA	Recurrent spontaneous abortion
NP	Normal pregnancy
FABP5	Fatty acid-binding protein 5
MRPL17	Mitochondrial ribosomal protein L17
HO-1	Heme oxygenase 1
ROS	Reactive oxygen species
TBHP	Tert-butyl hydroperoxide
ND2	NADH dehydrogenase subunit 2
ND4	NADH dehydrogenase subunit 4
ND4L	NADH dehydrogenase subunit 4L
CYTB	Cytochrome B
CYTC	Cytochrome C
MT-CO3	Mitochondrially encoded cytochrome c oxidase subunit III
SLE	Systemic lupus erythematosus
PFA	Paraformaldehyde
ECL	Enhanced chemiluminescence
CCK-8	Cell Counting Kit-8
MMP	Mitochondrial membrane potential
ELISA	Enzyme-linked immunosorbent assay
scRNA-seq	single-cell RNA sequencing
mtDNA	Mitochondrial DNA
MMPs	Matrix metalloproteinases
KEGG	Kyoto Encyclopedia of Genes and Genomes
NK	Natural killer
GSEA	Gene Set Enrichment Analysis
SRA	Sequence Read Archive
CS	Cell supernatant

References

[1] Practice Committee of the American Society for Reproductive Medicine, Evaluation and treatment of recurrent pregnancy loss: a committee opinion, *Fertil. Steril.* 98 (5) (2012) 1103–1111, <https://doi.org/10.1016/j.fertnstert.2012.06.048>.

[2] E. Dimitriadis, E. Menkhorst, S. Saito, W.H. Kuttah, J.J. Brosens, Recurrent pregnancy loss, *Nat. Rev. Dis. Primers* 6 (1) (2020) 98, <https://doi.org/10.1038/s41572-020-00228-z>.

[3] O.B. Christiansen, Special issue recurrent pregnancy loss: etiology, diagnosis, and therapy, *J. Clin. Med.* 10 (21) (2021) 5040, <https://doi.org/10.3390/jcm10215040>.

[4] X. Li, J. Shi, W. Zhao, X. Huang, L. Cui, L. Liu, et al., WNT16 from decidual stromal cells regulates HTR8/SVneo trophoblastic cell function via AKT/beta-catenin pathway, *Reproduction* 163 (2022) 241–250, <https://doi.org/10.1530/REP-21-0282>.

[5] B. Gellersen, J.J. Brosens, Cyclic decidualization of the human endometrium in reproductive health and failure, *Endocr. Rev.* 35 (6) (2014) 851–905, <https://doi.org/10.1210/er.2014-1045>.

[6] W. Wang, F. Vilella, P. Alama, I. Moreno, M. Mignardi, A. Isakova, et al., Single-cell transcriptomic atlas of the human endometrium during the menstrual cycle, *Nat. Med.* 26 (10) (2020) 1644–1653, <https://doi.org/10.1038/s41591-020-1040-z>.

[7] Y. Liang, S. Lai, L. Huang, Y. Li, S. Zeng, S. Zhang, et al., JAZF1 safeguards human endometrial stromal cells survival and decidualization by repressing the transcription of G0S2, *Commun. Biol.* 6 (1) (2023) 568, <https://doi.org/10.1038/s42003-023-04931-x>.

[8] W. Ma, M. Cao, S. Bi, L. Du, J. Chen, H.J. Wang, et al., MAX deficiency impairs human endometrial decidualization through down-regulating OSR2 in women with recurrent spontaneous abortion, *Cell Tissue Res.* 388 (2) (2022) 453–469, <https://doi.org/10.1007/s00441-022-03579-z>.

[9] L. Du, W. Deng, S. Zeng, P. Xu, L. Huang, Y. Liang, et al., Single-cell transcriptome analysis reveals defective decidual stromal niche attributes to recurrent spontaneous abortion, *Cell Prolif.* 54 (2021) e13125, <https://doi.org/10.1111/cpr.13125>.

[10] X. Liu, X. Wei, J. Wu, Y. Xu, J. Hu, C. Qin, et al., CBL1 promotes endometrial stromal cell senescence via inhibiting PTEN in recurrent spontaneous abortion, *FASEB (Fed. Am. Soc. Exp. Biol.) J.* 38 (14) (2024) e23833, <https://doi.org/10.1096/fj.202400972R>.

[11] K.H. Al-Gubory, P.A. Fowler, C. Garrel, The roles of cellular reactive oxygen species, oxidative stress and antioxidants in pregnancy outcomes, *Int. J. Biochem. Cell Biol.* 42 (2010) 1634–1650, <https://doi.org/10.1016/j.biocel.2010.06.001>.

[12] D.I. Chiarello, C. Abad, D. Rojas, F. Toledo, C.M. Vázquez, A. Mate, et al., Oxidative stress: normal pregnancy versus preeclampsia, *Biochim. Biophys. Acta, Mol. Basis Dis.* 1866 (2) (2020) 165354, <https://doi.org/10.1016/j.bbdis.2018.12.005>.

[13] E.H. Joo, Y.R. Kim, N. Kim, J.E. Jung, S.H. Han, H.Y. Cho, Effect of endogenous and exogenous oxidative stress triggers on adverse pregnancy outcomes: preeclampsia, fetal growth restriction, gestational diabetes mellitus and preterm birth, *Int. J. Mol. Sci.* 22 (18) (2021) 10122, <https://doi.org/10.3390/ijms221810122>.

[14] E. Jauniaux, A.L. Watson, J. Hempstock, Y.P. Bao, J.N. Skepper, G.J. Burton, Onset of maternal arterial blood flow and placental oxidative stress. A possible factor in human early pregnancy failure, *Am. J. Pathol.* 157 (6) (2000) 2111–2122, [https://doi.org/10.1016/S0002-9440\(10\)64849-3](https://doi.org/10.1016/S0002-9440(10)64849-3).

[15] H. Toy, H. Camuzcuoglu, A. Camuzcuoglu, H. Celik, N. Aksoy, Decreased serum prolidase activity and increased oxidative stress in early pregnancy loss, *Gynecol. Obstet. Invest.* 69 (2) (2010) 122–127, <https://doi.org/10.1159/000262608>.

[16] N. Sugino, M. Nakata, S. Kashida, A. Karube, S. Takiguchi, H. Kato, Decreased superoxide dismutase expression and increased concentrations of lipid peroxide and prostaglandin F(2alpha) in the decidua of failed pregnancy, *Mol. Hum. Reprod.* 6 (7) (2000) 642–647, <https://doi.org/10.1093/molehr/6.7.642>.

[17] H.H. Shen, C.J. Wang, X.Y. Zhang, Y.R. Sheng, S.L. Yang, Z.M. Zheng, et al., HIF1A-induced heme oxygenase 1 promotes the survival of decidual stromal cells against excess heme-mediated oxidative stress, *Reproduction* 163 (1) (2021) 33–43, <https://doi.org/10.1530/REP-21-0314>.

[18] Q. Lv, G. Wang, Y. Zhang, X. Han, H. Li, W. Le, et al., FABP5 regulates the proliferation of clear cell renal cell carcinoma cells via the PI3K/AKT signaling pathway, *Int. J. Oncol.* 54 (4) (2019) 1221–1232, <https://doi.org/10.3892/ijo.2019.4721>.

[19] W. Wang, Z. Liu, X. Chen, Y. Lu, B. Wang, F. Li, et al., Downregulation of FABP5 suppresses the proliferation and induces the apoptosis of gastric cancer cells through the Hippo signaling pathway, *DNA Cell Biol.* 40 (8) (2021) 1076–1086, <https://doi.org/10.1089/dna.2021.0370>.

[20] Y. Guo, Y. Liu, S. Zhao, W. Xu, Y. Li, P. Zhao, et al., Oxidative stress-induced FABP5 S-glutathionylation protects against acute lung injury by suppressing inflammation in macrophages, *Nat. Commun.* 12 (1) (2021) 7094, <https://doi.org/10.1038/s41467-021-27428-9>.

[21] S. Gao, G. Li, Y. Shao, Z. Wei, S. Huang, F. Qi, et al., FABP5 deficiency impairs mitochondrial function and aggravates pathological cardiac remodeling and dysfunction, *Cardiovasc. Toxicol.* 21 (8) (2021) 619–629, <https://doi.org/10.1007/s12012-021-09653-2>.

[22] Q. Guo, I. Kawahata, A. Cheng, H. Wang, W. Jia, H. Yoshino, et al., Fatty acid-binding proteins 3 and 5 are involved in the initiation of mitochondrial damage in

- ischemic neurons, *Redox Biol.* 59 (2023) 102547, <https://doi.org/10.1016/j.redox.2022.102547>.
- [23] K. Red-Horse, P.M. Drake, S.J. Fisher, Human pregnancy: the role of chemokine networks at the fetal-maternal interface, *Expet Rev. Mol. Med.* 6 (11) (2004) 1–14, <https://doi.org/10.1017/S1462399404007720>.
- [24] N.J. Hannan, R.L. Jones, C.A. White, L.A. Salamonsen, The chemokines, CXCL1, CCL14, and CCL4, promote human trophoblast migration at the feto-maternal interface, *Biol. Reprod.* 74 (5) (2006) 896–904, <https://doi.org/10.1095/biolreprod.105.045518>.
- [25] P.K. Lala, C. Chakraborty, Factors regulating trophoblast migration and invasiveness: possible derangements contributing to pre-eclampsia and fetal injury, *Placenta (Eastbourne)* 24 (6) (2003) 575–587, [https://doi.org/10.1016/s0143-4004\(03\)00063-8](https://doi.org/10.1016/s0143-4004(03)00063-8).
- [26] J.S. Fitzgerald, T.G. Poehlmann, E. Schleussner, U.R. Markert, Trophoblast invasion: the role of intracellular cytokine signalling via signal transducer and activator of transcription 3 (STAT3), *Hum. Reprod. Update* 14 (4) (2008) 335–344, <https://doi.org/10.1093/humupd/dmn010>.
- [27] N.M. Orsi, R.M. Tribe, Cytokine networks and the regulation of uterine function in pregnancy and parturition, *J. Neuroendocrinol.* 20 (4) (2008) 462–469, <https://doi.org/10.1111/j.1365-2826.2008.01668.x>.
- [28] M. Knöfler, Critical growth factors and signalling pathways controlling human trophoblast invasion, *Int. J. Dev. Biol.* 54 (2–3) (2010) 269–280, <https://doi.org/10.1387/ijdb.082769mk>.
- [29] M. Xiong, L. Li, L. Wen, A. Zhao, Decidual stromal cell-derived exosomes deliver miR-22-5p, R-1 to suppress trophoblast metabolic switching from mitochondrial respiration to glycolysis by targeting PDK4 in unexplained recurrent spontaneous abortion, *Placenta (Eastbourne)* 153 (2004) 1–21, <https://doi.org/10.1016/j.placenta.2024.05.131>.
- [30] H. Singh, Y. Endo, G. Nie, Decidual HtrA3 negatively regulates trophoblast invasion during human placentation, *Hum. Reprod.* 26 (4) (2011) 748–757, <https://doi.org/10.1093/humrep/der019>.
- [31] M.Q. Li, X.F. Hou, J. Shao, C.L. Tang, D.J. Li, The DSCs-expressed CD82 controls the invasiveness of trophoblast cells via integrin β 1/MAPK/MAPK3/1 signaling pathway in human first-trimester pregnancy, *Biol. Reprod.* 82 (5) (2010) 968–979, <https://doi.org/10.1095/biolreprod.109.080739>.
- [32] S. Kumaravel, S. Singh, S. Roy, L. Venkatasamy, T.K. White, S. Sinha, et al., CXCL11-CXCR3 Axis mediates tumor lymphatic cross talk and inflammation-induced tumor, promoting pathways in head and neck cancers, *Am. J. Pathol.* 190 (4) (2020) 900–915, <https://doi.org/10.1016/j.ajpath.2019.12.004>.
- [33] M. Puchert, J. Obst, C. Koch, K. Zieger, J. Engeler, CXCL11 promotes tumor progression by the biased use of the chemokine receptors CXCR3 and CXCR7, *Cytokine* 125 (2020) 154809, <https://doi.org/10.1016/j.cyto.2019.154809>.
- [34] H.J. Hwang, Y.R. Lee, D. Kang, H.C. Lee, H.R. Seo, J.K. Ryu, et al., Endothelial cells under therapy-induced senescence secrete CXCL11, which increases aggressiveness of breast cancer cells, *Cancer Lett.* 490 (2020) 100–110, <https://doi.org/10.1016/j.canlet.2020.06.019>.
- [35] S. Ali, S. Majid, M. Niamat Ali, S. Taing, H.A. El-Serehy, F.A. Al-Misned, Evaluation of etiology and pregnancy outcome in recurrent miscarriage patients, *Saudi J. Biol. Sci.* 27 (10) (2020) 2809–2817, <https://doi.org/10.1016/j.sjbs.2020.06.049>.
- [36] D. Croxatto, P. Vacca, F. Canegallo, R. Conte, P.L. Venturini, L. Moretta, et al., Stromal cells from human decidua exert a strong inhibitory effect on NK cell function and dendritic cell differentiation, *PLoS One* 9 (2) (2014) e89006, <https://doi.org/10.1371/journal.pone.0089006>.
- [37] H. Lu, H.L. Yang, W.J. Zhou, Z.Z. Lai, X.M. Qiu, Q. Fu, et al., Rapamycin prevents spontaneous abortion by triggering decidual stromal cell autophagy-mediated NK cell residence, *Autophagy* 17 (9) (2021) 2511–2527, <https://doi.org/10.1080/15548627.2020.1833515>.
- [38] W.T. Hu, L.L. Huang, M.Q. Li, L.P. Jin, D.J. Li, X.Y. Zhu, Decidual stromal cell-derived IL-33 contributes to Th2 bias and inhibits decidual NK cell cytotoxicity through NF- κ B signaling in human early pregnancy, *J. Reprod. Immunol.* 109 (2015) 52–65, <https://doi.org/10.1016/j.jri.2015.01.004>.
- [39] T. Llorca, M.J. Ruiz-Magaña, R. Martínez-Aguilar, O.M. García-Valdeavero, L. Rodríguez-Doña, A.C. Abadía-Molina, et al., Decidualized human decidual stromal cells inhibit chemotaxis of activated T cells: a potential mechanism of maternal-fetal immune tolerance, *Front. Immunol.* 14 (2023) 1223539, <https://doi.org/10.3389/fimmu.2023.1223539>.
- [40] T. Nagamatsu, D.J. Schust, J. Sugimoto, B.F. Barrier, Human decidual stromal cells suppress cytokine secretion by allogenic CD4+ T cells via PD-1 ligand interactions, *Hum. Reprod.* 24 (12) (2009) 3160–3171, <https://doi.org/10.1093/humrep/dep308>.
- [41] L. Wang, H. Wang, J. Luo, T. Xie, G. Mor, A. Liao, Decorin promotes decidual M1-like macrophage polarization via mitochondrial dysfunction resulting in recurrent pregnancy loss, *Theranostics* 12 (17) (2022) 7216–7236, <https://doi.org/10.7150/thno.78467>.
- [42] Y. Lou, M. Hu, Q. Wang, M. Yuan, N. Wang, F. Le, et al., Estradiol suppresses TLR4-triggered apoptosis of decidual stromal cells and drives an anti-inflammatory Th2 shift by activating SGK1, *Int. J. Biol. Sci.* 13 (4) (2017) 434–448, <https://doi.org/10.7150/ijbs.18278>.
- [43] S. Wang, C. Cao, H. Piao, Y. Li, Y. Tao, X. Zhang, et al., Tim-3 protects decidual stromal cells from toll-like receptor-mediated apoptosis and inflammatory reactions and promotes Th2 bias at the maternal-fetal interface, *Sci. Rep.* 5 (2015) 9013, <https://doi.org/10.1091/mbc.E17-04-0239>.
- [44] J.M. Box, J. Kaur, R.A. Stuart, MrpL35, a mitospecific component of mitochondria, plays a key role in cytochrome c oxidase assembly, *Mol. Biol. Cell* 28 (24) (2017) 3489–3499, <https://doi.org/10.1091/mbc.E17-04-0239>.
- [45] A.K. Rai, S. Sanghvi, N.S. Muthukumaran, D. Chandrasekera, A. Kadam, J. Kishore, et al., Role of mitochondrial ribosomal protein L7/L12 (MRPL12) in diabetic ischemic heart disease, *Free Radic. Biol. Med.* 222 (2024) 531–538, <https://doi.org/10.1016/j.freeradbiomed.2024.07.003>.
- [46] Y. Han, Y. Liu, J. Zhen, S. Hou, B. Zhang, Z. Cui, et al., P53 regulates mitochondrial biogenesis via transcriptional induction of mitochondrial ribosomal protein L12, *Exp. Cell Res.* 418 (1) (2022) 113249, <https://doi.org/10.1016/j.yexcr.2022.113249>.
- [47] Y.V. Surovtseva, T.E. Shutt, J. Cotney, H. Cimen, S.Y. Chen, E.C. Koc, et al., Mitochondrial ribosomal protein L12 selectively associates with human mitochondrial RNA polymerase to activate transcription, *Proc. Natl. Acad. Sci. U.S.A.* 108 (44) (2011) 17921–17926, <https://doi.org/10.1073/pnas.1108852108>.
- [48] S. Bakhshalizadeh, D.H. Hock, N.A. Siddall, B.L. Kline, R. Sreenivasan, K.M. Bell, et al., Deficiency of the mitochondrial ribosomal subunit, MRPL50, causes autosomal recessive syndromic premature ovarian insufficiency, *Hum. Genet.* 142 (7) (2023) 879–907, <https://doi.org/10.1007/s00439-023-02563-z>.
- [49] H.B. Li, R.X. Wang, H.B. Jiang, E.D. Zhang, J.Q. Tan, H.Z. Xu, et al., Mitochondrial ribosomal protein L10 associates with cyclin B1/cdk1 activity and mitochondrial function, *DNA Cell Biol.* 35 (11) (2016) 680–690, <https://doi.org/10.1089/dna.2016.3271>.
- [50] H. Ke, S. Dass, J.M. Morrissey, M.W. Mather, A.B. Vaidya, The mitochondrial ribosomal protein L13 is critical for the structural and functional integrity of the mitochondrion in *Plasmodium falciparum*, *J. Biol. Chem.* 293 (21) (2018) 8128–8137, <https://doi.org/10.1074/jbc.RA118.002552>.
- [51] J. Zhang, G. He, X. Jin, B.T. Alenezi, A.A. Naeem, S.A. Abdulsamad, et al., Molecular mechanisms on how FAPB5 inhibitors promote apoptosis-induction sensitivity of prostate cancer cells, *Cell Biol. Int.* 47 (5) (2023) 929–942, <https://doi.org/10.1002/cbin.11989>.
- [52] C. Gordon, J. Trainor, R.J. Shah, K. Studholme, A. Gelman, F. Doswell, et al., Fatty acid binding protein 5 inhibition attenuates pronociceptive cytokine/chemokine expression and suppresses osteoarthritis pain: a comparative human and rat study, *Osteoarthr. Cartil.* 32 (3) (2024) 266–280, <https://doi.org/10.1016/j.joca.2023.11.010>.
- [53] J. Hao, J. Yu, M.S. Yorek, C.L. Yu, R.M. Pope, M.S. Chimenti, et al., Keratinocyte FAPB5-VCP complex mediates recruitment of neutrophils in psoriasis, *Cell Rep.* 42 (11) (2023) 113449, <https://doi.org/10.1016/j.celrep.2023.113449>.
- [54] D. Yin, J. Hao, R. Jin, Y. Yi, S.R. Bodduluri, Y. Hua, et al., Epidermal fatty acid-binding protein mediates depilatory-induced acute skin inflammation, *J. Invest. Dermatol.* 142 (7) (2022) 1824–1834.e7, <https://doi.org/10.1016/j.jid.2021.11.040>.
- [55] X. Wu, L.Y. Cheong, L. Yuan, L. Jin, Z. Zhang, Y. Xiao, et al., Islet-resident memory T cells orchestrate the immunopathogenesis of type 1 diabetes through the FAPB4-CXCL10 Axis, *Adv. Sci.* 11 (30) (2024) e2308461, <https://doi.org/10.1002/adv.202308461>.